Materials Letters 349 (2023) 134835

Contents lists available at ScienceDirect

Materials Letters

journal homepage: www.elsevier.com/locate/matlet

Tailoring the crystallographic texture of biomedical metastable β-type Ti-alloy produced via laser powder bed fusion using temperature-field simulations

Takuya Ishimoto [a,b,c], Ryoya Suganuma [a], Takayoshi Nakano [a,b,*]

[a] Division of Materials and Manufacturing Science, Graduate School of Engineering, Osaka University, 2-1 Yamadaoka, Suita, Osaka 565-0871, Japan
[b] Anisotropic Design and Additive Manufacturing Research Center, Osaka University, 2-1, Yamadaoka, Suita, Osaka 565-0871, Japan
[c] Aluminium Research Center, University of Toyama, 3190, Gofuku, Toyama, Toyama 930-8555, Japan

ARTICLE INFO

Keywords:
Laser powder bed fusion
Crystallographic texture
Single crystal
Polycrystal
Temperature simulation

ABSTRACT

Recently, the use of laser powder bed fusion (LPBF) to create crystallographic textures, such as single-crystal-like and polycrystalline textures, has attracted attention. However, the relationship between the LPBF conditions and the resulting texture is unclear. This study investigates the effects of the LPBF conditions (laser power and scanning speed) on the texture by estimating the solidification behavior using temperature-field simulations. Herein, we show for the first time that laser power and scanning speed negatively and positively affect the solidification rate R, respectively, and do not affect the thermal gradient G significantly. Thus, when the laser power decreases and scanning speed increases, the G/R ratio decreases and polycrystal formation is enhanced. This is consistent with practical observations.

1. Introduction

Laser powder bed fusion (LPBF) has attracted attention for controlling crystallographic textures [1,2]. Several strategies have been attempted for texture control [3], including adjusting process parameters, devising laser scanning strategies, and modifying laser energy distribution. Among these methods, this study focuses on process variables with a wide range of selectivity. Various textures have been produced by changing process parameters such as the laser power, laser scanning speed, hatch distance, and layer thickness [4–6]; however, they have mainly been determined via trial and error. Therefore, a quantitative evaluation of the effect of each parameter on the crystallographic texture is expected to provide guidelines for controlling the texture.

This study fabricated β-type Ti-15Mo-5Zr-3Al alloy products using different laser conditions and analyzed their crystallographic textures. In addition, a numerical simulation of the temporal and spatial temperature distributions under change of laser power and scanning speed was performed to clarify the parameters governing the variation in crystallographic texture and quantitatively evaluate the magnitude of the contribution of these parameters.

2. Experimental procedures

Ti-15Mo-5Zr-3Al gas-atomized powder (D50 = 26 μm) was obtained from Osaka Titanium Technologies (Japan). Specimens measuring 5 × 5 × 10 mm^3 were fabricated using an EOS M290 (EOS, Germany) and scan strategy X, where the laser scanned bidirectionally along the x-axis under an Ar atmosphere. The build direction was the z-direction. Samples were produced under two conditions. The laser power and scanning speed under conditions A and B were 360 W and 1200 mm/s and 180 W and 1400 mm/s, respectively. The layer thickness and scanning pitch were fixed at 60 and 100 μm, respectively. The microstructures were investigated using optical microscopy, field-emission scanning electron microscopy (JIB-4610F, JEOL, Japan), and electron backscatter diffraction (NordlysMax^3, Oxford Instruments, UK).

Melting and solidification during LPBF were analyzed by calculating the heat transfer and temperature changes in COMSOL Multiphysics® 5.5 (COMSOL, USA) using the finite element method. The model had base dimensions of 5 × 5 mm^2, and it was divided into a tetrahedral mesh. Detailed calculation conditions and the thermophysical properties used can be found elsewhere [7].

In brief, the heat generated by the laser was modeled as a Gaussian

* Corresponding author at: Division of Materials and Manufacturing Science, Graduate School of Engineering, Osaka University, 2-1 Yamadaoka, Suita, Osaka 565-0871, Japan.
E-mail address: nakano@mat.eng.osaka-u.ac.jp (T. Nakano).

https://doi.org/10.1016/j.matlet.2023.134835
Received 7 April 2023; Received in revised form 7 June 2023; Accepted 27 June 2023
Available online 28 June 2023

function distributed in the x–y plane that decayed in the z-direction [7]. The temperature variations owing to the laser scan under the conditions shown in Table 1 were calculated based on heat conduction to the fabricating part and heat transfer to the surrounding environment. Based on the simulation, the temperature gradient G [K/m], solidification rate R [m/s], and cooling rate $\dot{T}$ [K/s] were calculated using $G = |\nabla T|$, $\dot{T} = \mathrm{d}T/\mathrm{d}t$, and $R = \dot{T}/G$.

3. Results and discussion

The inverse pole figures and corresponding pole figures for the specimens are shown in Fig. 1(a, b). The texture depended on the manufacturing parameters. Condition A produced a strong crystallographic texture with the {0 1 1} and {1 0 0} planes preferentially orientated in the z- and x-directions, respectively. This texture generated under the scan strategy X was caused by the two directional growths of ⟨1 0 0⟩ within the melt pool cross-section at angles of ±45° from the build direction [8], as illustrated in Supplementary Fig. 1S. By contrast, condition B produced a highly random polycrystalline texture, despite using the same scan strategy as Condition A, suggesting the influence of laser irradiation conditions. The optical images of the upper parts of the samples are shown in Fig. 1(c, d). Under condition A, a deeply penetrating keyhole-type pool was produced. Under condition B, the melt pool was shallower and narrower because the input heat energy was reduced by ~43%. Under condition A, the top 60% of the melt pool was overwritten (remelted) when the next layer was irradiated. By contrast, under condition B, the majority of the melt pool was not overwritten, thus producing some lack-of-fusion-type pores.

Fig. 2(a) shows a G–R distribution map of the melt pool during solidification based on the numerical calculations; the columnar-to-equiaxed transition (CET) line for Ti-6Al-4V [9] is shown for reference. The temperature difference between the liquidus and solidus lines ΔT of Ti-15Mo-5Zr-3Al was 20 K [10], which was smaller than that of Ti-6Al-4V (50 K) [11]; therefore, the CET line of Ti-15Mo-5Zr-3Al was expected to be lower than that of Ti-6Al-4V. Under condition B, the plots were distributed higher on the R-axis than under condition A.

Fig. 2(b, c) shows the G/R within the melt pool when each point solidified. Under condition A (Fig. 2(b)), the pink and blue regions (high and medium G/R, respectively) cover the majority of the melt pool, and the pink region accounts for ~40% of the total region from the bottom remaining unaffected by the next layer. Under condition B (Fig. 2(c)), a light-blue region (low G/R) exists in the center of the melt pool, corresponding to the relatively large R. Lower G/R ratios indicate that compositional undercooling is more likely and possible loss of the smooth solid–liquid interface. Consequently, nucleation may form equiaxed grains and unstable dendrites [12], producing a more random texture. This is consistent with the disordered polycrystals formed under condition B, where R was large and G/R was small. Light-blue regions with smaller G/R are also observed under condition A; however, they are remelted when the next layer is irradiated. Consequently, the crystal orientation can be inherited by subsequent melt pools via epitaxial growth. The crystallographic orientation can be stabilized by reducing the crystallographic misorientation at the center of the melt pool, where the solid–liquid interfaces migrate from either side [13,14].

The G and R distributions affect the texture but cannot be controlled directly during LPBF. Therefore, simulations were performed with an identical heat source to analyze the effects of the laser power P and scanning speed v (controllable parameters) on G and R. The values of P and v are summarized in Table 1. Fig. 3(a, b) shows the G and R distributions when the scanning speed was constant at 1200 mm/s and the laser power was varied and when the laser power was constant at 180 W and the scanning speed was varied. Multiple regression analysis was performed with P and v as the explanatory variables and averaged G and R as the objective variables. The resulting standardized partial regression coefficients β and p-values are shown in Fig. 3(c, d). For G, the p-values of P and v exceeded 0.05, indicating no significant effects. For R, the β coefficients of P and v were -0.77 ($p = 0.0055$) and 0.53 ($p = 0.016$), indicating significant negative and positive effects on R, respectively. Hence, R increased as the input energy density decreased. Furthermore, the laser power had a greater effect on R than the scanning speed.

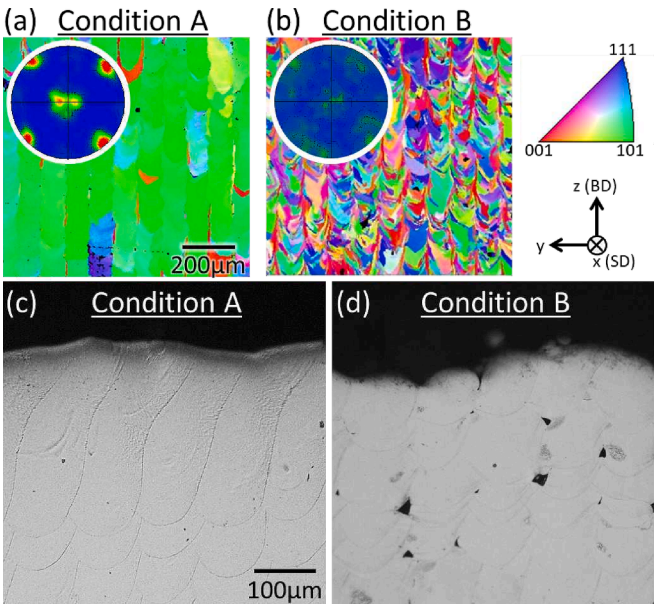

Fig. 1. Cross sections of the specimens in the y–z plane. (a, b) Inverse pole figures and corresponding pole figures of the specimens. (c, d) Optical images of the upper parts of the specimens.

Besides P and v, hatch distance [15] and hatch length [16] have been reported to affect G and R and thus crystallographic texture. Analysis of the effects of these and other elements in the LPBF fabrication condition on G and R using numerical simulation is expected to help establish a strategy for texture control. In addition, the use of heat treatment under stress as a post-process may possibly improve the strength of the poorly organized texture [17].

Thus, the crystallographic texture is affected by the laser power and scanning speed via the thermal gradient and solidification rate. To obtain a strong texture, the energy density must be high (i.e., the laser power and scanning speed must be sufficiently high and low, respectively).

Table 1
Fabrication parameters used in the simulation.

Title	P [W]	v [mm/s]
P1	540	1200
P2	360	1200
P3	180	1200
V1	180	600
V2	180	1200
V3	180	2000

4. Conclusion

Strong or highly random crystallographic textures were obtained in the Ti-15Mo-5Zr-3Al under different fabrication conditions via LPBF. Numerical simulations revealed that R increased with decreasing P or increasing v, that is, with decreasing input energy density. Smaller P and larger v resulted in smaller G/R and enhanced polycrystal formation.

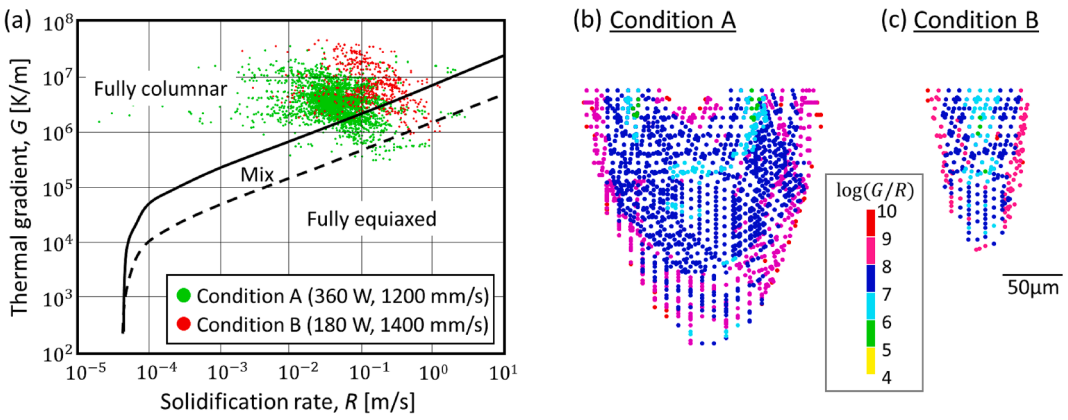

Fig. 2. Melt-pool analysis. (a) Solidification (*G*–*R*) map based on the simulation (CET line for Ti-6Al-4V for reference) [9]. (b, c) *G*/*R* distribution maps of the melt pools.

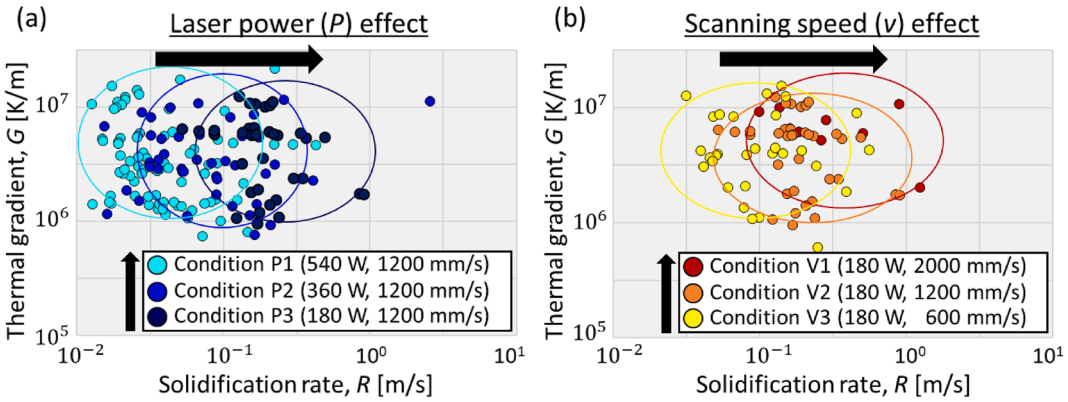

(c) Laser power (*P*) effect

Thermal gradient (*G*)		Solidification rate (*R*)	
β	*p*	*β*	*p*
-0.66	0.12	-0.77	0.0055

(d) Scanning speed (*v*) effect

Thermal gradient (*G*)		Solidification rate (*R*)	
β	*p*	*β*	*p*
0.47	0.22	0.53	0.016

Fig. 3. Simulations analyzing the effects of laser power and scanning speed. (a, b) Variations in the *G*–*R* distribution as a function of the manufacturing conditions. (c, d) Multiple regression analysis representing the effects of *P* and *v* on *G* and *R*.

CRediT authorship contribution statement

Takuya Ishimoto: Investigation, Methodology, Formal analysis, Writing – original draft. **Ryoya Suganuma:** Investigation, Visualization. **Takayoshi Nakano:** Conceptualization, Supervision, Project administration, Writing – review & editing.

Declaration of Competing Interest

The authors declare that they have no known competing financial interests or personal relationships that could have appeared to influence the work reported in this paper.

Data availability

Data will be made available on request.

Acknowledgments

Funding: This work was supported by CREST-Nanomechanics [JPMJCR2194] from the Japan Science and Technology Agency, a Grant-in-Aid for Transformative Research Area (A) [JP21H05197] and a Grant-in-Aid for Scientific Research [JP23H01234] from the Japan Society for the Promotion of Science. TI was supported by research funding from the Light Metal Educational Foundation and a 1st Frontier Research Grant from the Japan Institute of Metals and Materials.

Appendix A. Supplementary data

Supplementary data to this article can be found online at https://doi.org/10.1016/j.matlet.2023.134835.

References

[1] N.T. Andani, et al., Mater. Lett. 340 (2023), 134156.
[2] K. Hagihara, T. Nakano, JOM 74 (2022) 1760–1773.
[3] W.A. de Morais, F.J.G. Landgraf, Tecnol. Metal. Mater. Min. 20 (2023) e2802.
[4] S.H. Sun, et al., Addit. Manuf. 47 (2021), 102329.
[5] O. Gokcekaya, et al., Mater. Res. Lett. 11 (2023) 274–280.
[6] O. Gokcekaya, et al., Acta Mater. 212 (2021), 116876.
[7] A. Takase, et al., Addit. Manuf. 47 (2021), 102257.
[8] T. Ishimoto, et al., Scr. Mater. 132 (2017) 34–38.
[9] P.A. Kobryn, et al., J. Mater. Process. Tech. 135 (2003) 330–339.
[10] A. Takase, et al., Scr. Mater. 201 (2021), 113953.
[11] R. Rai, et al., J. Phys. D: Appl. Phys. 42 (2008), 025503.
[12] J.D. Hunt, Mater. Sci. Eng. 65 (1984) 75–83.
[13] T. Todo, et al., Scr. Mater. 206 (2022), 114252.

[14] T. Ishimoto, et al., Addit. Manuf. 43 (2021), 102004.
[15] S.E. Saghaian, et al., Opt. Laser Technol. 149 (2022), 107680.
[16] N. Nadammal, et al., Mater. Des. 134 (2017) 139–150.
[17] C. Gao, et al., Addit. Manuf. 68 (2023), 103516.